applied sciences

MDPI

Article

Quasi-CW Pumping of a Single-Frequency Fiber Amplifier for Efficient SHG in PPLN Crystals with Reduced Thermal Load

Enkeleda Balliu [1,*], Magnus Engholm [1], Michel J. F. Digonnet [2] and Hans-Erik Nilsson [3]

[1] Department of Electronics, Mid Sweden University, 851 70 Sundsvall, Sweden; magnus.engholm@miun.se
[2] Applied Physics Department, Stanford University, Stanford, CA 94305, USA
[3] Faculty of Science, Mid Sweden University, 851 70 Sundsvall, Sweden; Hans-Erik.Nilsson@miun.se
* Correspondence: enkeleda.balliu@miun.se

Abstract: Single-frequency lasers are essential for high-resolution spectroscopy and sensing applications as they combine high-frequency stability with low noise and high output power stability. For many of these applications, there is increasing interest in power-scaling single-frequency sources, both in the near-infrared and visible spectral range. We report the second-harmonic generation of 670 µJ at 532 nm of a single-frequency fiber amplifier signal operating in the quasi-continuous-wave mode in a 10-mm periodically poled Mg-doped lithium niobate (MgO:PPLN) crystal, while increasing compactness. To the best of our knowledge, this is the highest pulse energy generated in this crystal, which may find applications in the visible and UV such as remote Raman spectroscopy.

Keywords: quasi-CW; single-frequency; SBS; thermal load; compact; SHG; PPLN crystal; compact

Citation: Balliu, E.; Engholm, M.; Digonnet, M.J.F.; Nilsson, H.-E. Quasi-CW Pumping of a Single-Frequency Fiber Amplifier for Efficient SHG in PPLN Crystals with Reduced Thermal Load. *Appl. Sci.* **2022**, *12*, 285. https://doi.org/10.3390/app12010285

Academic Editor: Kijoon Lee

Received: 18 November 2021
Accepted: 21 December 2021
Published: 28 December 2021

1. Introduction

High-power single-frequency laser systems have become increasingly attractive thanks to their high spatial and temporal coherence, which has enabled technological advances in many applications such as high-resolution spectroscopy, remote sensing, non-linear frequency conversion, and holography. In particular, remote Raman spectroscopy [1,2] is witnessing increasing use, especially in military and defense applications, to detect and identify chemical, biological, radiological, nuclear, or explosive materials [3]. The Raman signal strength (intensity) is directly proportional to the power of the laser used to excite the sample, and inversely proportional to the laser wavelength [4]. In this regard, diode-pumped solid-state lasers are desirable laser sources, as they offer low noise, good power stability, and good beam pointing stability. Power scaling of single-frequency laser sources at 532 nm is, therefore, very attractive. It can be achieved by power scaling the signal at 1064 nm and/or increasing the efficiency of second-harmonic generation.

The former solution raises significant challenges that worsen with increasing compactness. The reason is that the combination of high power, small fiber core, and narrow spectral linewidth usually results in the onset of stimulated Brillouin scattering (SBS) [5] and, to a smaller extent, other undesirable power-scaling limitation effects occurring in the fiber, such as high thermal loading [6] and photodarkening [7]. SBS is generated by the non-linear interaction of the laser signal and the Stokes fields through an acoustic wave generated in the fiber through electrostriction [8,9]. When the optical power exceeds a certain power threshold $P_{cr,SBS}$, a strong frequency-shifted, backward-propagating wave is generated in the fiber, causing power instability. The SBS threshold power is proportional to the fiber core area and inversely proportional to the fiber length. Therefore, to power scale the signal at 1064 nm, we have chosen to use highly Yb-doped fibers, which contributes to both suppressing SBS and maintaining compactness [7].

On the other end, the generation of high single-frequency powers in the visible range in a simple and compact format is possible by using periodically-poled nonlinear crystals in a single-pass configuration. This solution is particularly important for single-frequency

lasers, because it can provide high conversion efficiencies even at limited fundamental powers (see Table 1). Even though periodically poled Mg-doped lithium niobate (MgO:PPLN) has a higher effective nonlinear optical coefficient ($d_{eff} \approx 16$ pm/V) [10] than PPKTP ($d_{eff} \approx 10$ pm/V) and PPLT ($d_{eff} \approx 9$ pm/V) [11], its lower thermal conductivity (4.4 W/(mK) [12] makes it less beneficial at high optical power. Nevetheless, a conversion efficiency of 34% and an output power 3 W at 532 nm were demonstrated by Furuya et al. [13] using a single-pass configuration. Lai et al. [14] reported 30% and 7.5 W in the same configuration. A higher conversion efficiency of 66% was demonstrated by Mizushima et al., who reported an output power of 5 W using a multi-pass scheme instead [15]. These three reports all used a crystal length of 25 mm and CW excitation. In most reports of green generation in the CW mode using PPLN crystals and both a fundamental power higher than 7 W and an output power higher than 2.5 W at 532 nm [10,16–18], gives rise to green-induced infrared absorption (GRIIRA). This effect causes damage to the material [19] and other thermal limitations such as thermal dephasing and thermal lensing, resulting in constraints of the conversion efficiency and deterioration of the generated beam quality.

One way to overcome the thermal limitations is to operate the laser in a pulsed mode. Second-harmonic generation benefits significantly from this approach, in two ways. First, for the same average signal power, the signal peak power can be significantly higher, resulting in a higher SHG power (proportional to the signal power squared). Second, for the same average power, the thermal load on both the fiber and the non-linear crystal are the same. Stated differently, the SHG efficiency is enhanced, but the thermal load is unchanged. Conversely, the same SHG conversion efficiency can be achieved with a lower average power and, therefore, a lower thermal load. These features can be advantageous to other applications such as remote pulsed Raman spectroscopy [20], metal laser cutting [21], and gas tracing [22], especially when the pulses are sufficiently long to maintain a similar behavior as in the CW mode.

Although conversion efficiencies of 68% [23] and 60% [24] have been demonstrated in pulsed mode operation in a PPLN crystal. The conversion efficiencies are high due to the short pulse duration, in the order of 100 ps [23] and 560 ps [24], while the second-harmonic pulse energies were relatively low, in the range of sub-μJ [23] to tens of μJ [24]. On the other hand, for a given drive current, operating a laser in the QCW mode generally allows it to be driven above its CW rating and to obtain peak powers that are greater than the maximum CW power. This approach has proven useful to increase the conversion efficiency in other non-linear crystals like LBO [25]. In general, short fundamental pulses (nanoseconds) produce high conversion efficiencies thanks to their very high peak powers, but low second-harmonic pulse energies due to their low pulse energy. Longer fundamental pulses yield the opposite benefits, namely lower efficiencies but higher second-harmonic pulse energies. In spite of this benefit, the use of longer pulses has not been fully exploited in a MgO:PPLN crystal. To the best of our knowledge, the highest pulse energy reported so far is limited to 440 μJ in a 20-mm MgO:PPLN crystal (double the length used in the work reported here), with no details on the development of QCW opereration [26].

Table 1. Selected work on the second-harmonic generation using periodically poled Mg-doped lithium niobate (MgO:PPLN) crystals.

Reference	Fundamental Power (W)	Pulse Energy at 1064 nm	Output Power at 532 nm (W)	Peak Power at 532 nm (W)	Conversion Efficiency (%)	Crystal Length (mm)	Configuration	Operation Mode
[14]	25	-	7.5	-	30	25	single-pass	CW
[15]	7.6	-	5	-	66	-	multi-pass	CW
[18]	20	-	1.1	-	9	10	single-pass	CW
[23]	0.2	-	0.135	-	68	10	single-pass	pulsed
[24]	0.069	10	0.04	-	60	5	single-pass	Pulsed
[26]	-	-	-	8.8	34	20	single-pass	QCW
This work	0.428	4280	0.067	6.7	20	10	single-pass	QCW

In light of the foregoing, here we investigate the frequency doubling of a QCW single-frequency fiber amplifier in a 10-mm MgO:PPLN crystal. We report the generation of

output peak powers at 1064 nm up to twice as high as the maximum power achievable under the CW pumping, and output pulse energies at 532 nm close to 700 µJ. To the best of our knowledge, this is the highest pulse energy achieved in a PPLN crystal. Moreover, QCW operation reduces the number of pump diodes required for the fundamental laser, hence contributing to further reducing the size of the fiber amplifier.

2. Experimental Setup

The experimental setup of the fiber amplifier used in this work is shown in Figure 1. The seed laser is a low-noise, single-frequency, diode-pumped solid-state laser (DPSSL) (Cobolt, a Hübner Company, Stockholm, Sweden), described in detail elsewhere [5]. Light from the seed source was free-space-coupled with a coupling efficiency into a single-cladding polarization-maintaining (PM) fiber greater than 85%. This fiber was spliced to a high-power PM isolator (Advanced Fiber Resources, Beijing, China), which was itself spliced to a (2 + 1) × 1 PM combiner (ITF Technologies, Quebec, CA, USA).

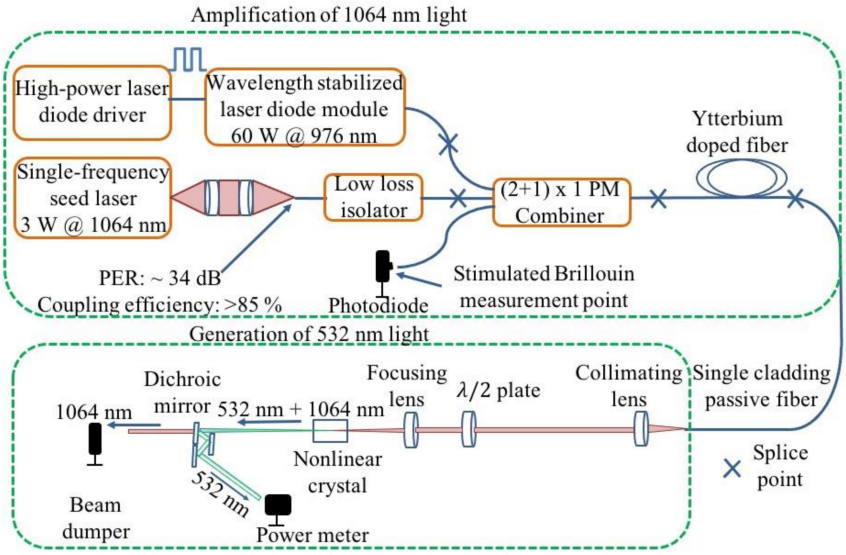

Figure 1. The schematic of the QCW fiber amplifier divided into two parts: the upper block depicts the QCW single-stage fiber amplifier. All components use the same 10/125-µm polarization-maintaining fiber; the lower block is a schematic representation of the single-pass frequency conversion to 532 nm.

A high pump-power stability was achieved by using a wavelength-stabilized pump-diode module (BWT Beijing, China) operating at 976 nm. It delivered up to 60 W of CW power at the maximum current rating of 12 A. A high-power, compact laser driver (DAE-20050, Monocrom, Barcelona, Spain) was used to control the pump diodes in either the CW or QCW mode. The active fiber used is the commercially available PM Yb-doped fiber with the highest Yb concentration (Liekki Yb1200-10/125DC-PM). It has a core/cladding diameter of 10/125 µm, and a core numerical aperture of 0.08, making it single-moded at 1064 nm. It has a cladding absorption of 6.5 dB/m at 976 nm. The fiber was coiled to a diameter of 8 cm. The unabsorbed pump power was stripped by a single-cladding PM passive fiber with the same core/cladding dimensions that was spliced to the end of the active fiber, with the possibility of replacing it with an anti-reflective end-cap in the future. The SBS signal power was monitored in the backward direction by a photodiode (see Figure 1). The onset of SBS was defined as the signal power at which the backward-propagating pulses started to deform and exhibit narrow spikes.

For single-pass external cavity nonlinear frequency conversion, we evaluated the performance of a 10-mm periodically poled MgO-doped $LiNbO_3$ (MgO:PPLN) crystal (Covesion, Southampton, UK) that was kept at constant temperature in a temperature-controlled oven. The crystal temperature was adjusted to achieve quasi-phase matching

and thereby maximize the conversion efficiency. No interface material such as thermal paste or copper foil was used to facilitate heat exchange between the crystal and the oven atmosphere. Three dichroic mirrors were placed after the non-linear crystal to remove the residual 1064 nm light from the frequency-converted 532-nm light. The power transmission value of the mirrors was nearly 98–99%, and consequently more than one mirror was needed. The maximum residual fundamental power was, therefore, at most ~0.001% (or less than 0.4 mW).

3. Experimental Results

3.1. High-Power Laser Diode Driver Performance in CW and QCW Modes

The laser driver produced a current waveform that could be either CW, modulated, or pulsed, up to a current of 200 A. In our experiments, we used diode currents up to 12 A in the CW mode, which is the rated maximum current of the pump laser diode in the CW mode. At this power, the diode produced an output power of 60 W (see Figure 2). The pump diodes were very stable, and wavelength-stabilized.

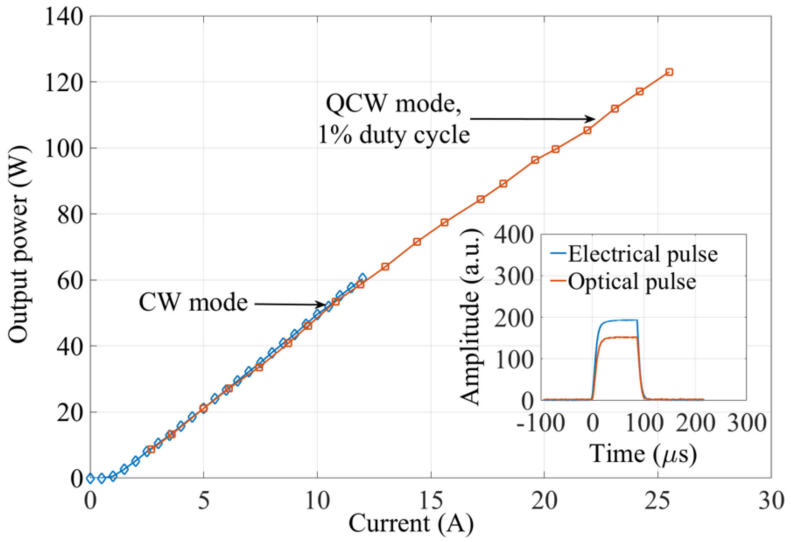

Figure 2. The output power of the wavelength-stabilized pump-diode module operating in the CW (average power) and QCW modes (peak power). Inset: Electrical and optical pulse shape of the pump-diode module.

However, in the QCW mode, a 100-µs pulse duration and a duty cycle of 1% were used, corresponding to a pulse repetition rate of 0.1 kHz. The maximum current that could be used was then more than twice the manufacturer's CW rating. Specifically, and as shown in Figure 2, we were able to drive the laser diode up to 25.5 A and produce a peak power of 123 W. The diode efficiency was nominally the same in the QCW and CW modes: operating it in the pulsed mode enabled us to extract twice as much power from it. The laser diode's output power was monitored for several hours at these settings and showed no sign of power degradation or thermal damage to the pump source, indicating that potentially higher diode currents or longer pulse durations could have been used. Nevertheless, this pump current was deemed sufficient for the purpose of this study.

3.2. Optimisation of the Yb-Doped Fiber Amplifier Output Power

Figure 3 presents the measured output-power characteristics of the single-frequency fiber amplifier. The amplifier was tested with different fiber lengths to identify the length that strikes a suitable compromise between the slope efficiency (which improves with increasing length) and the SBS power threshold (which decreases, i.e., degrades, with increasing length).

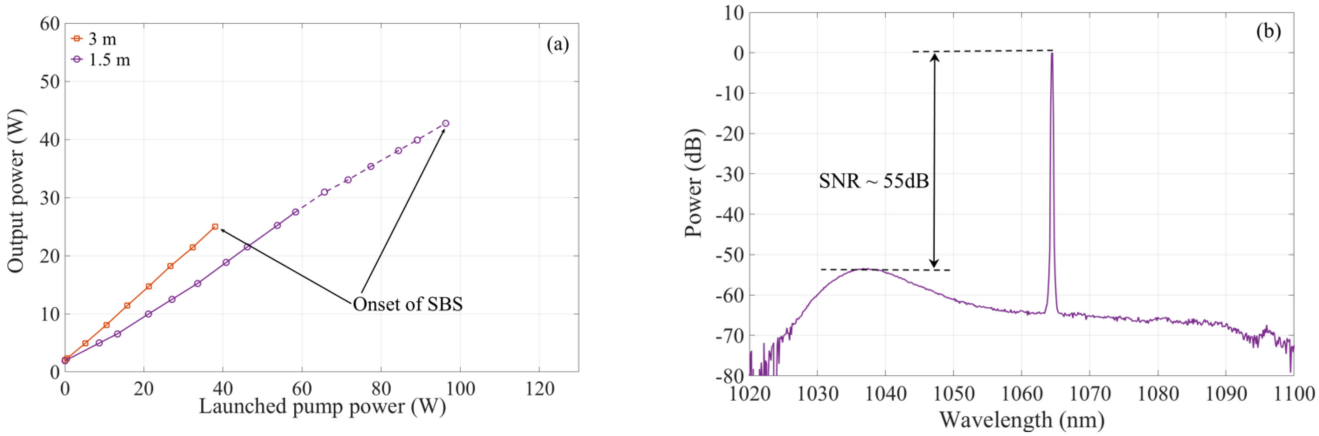

Figure 3. Measured characteristics of the single-stage fiber amplifier output signal at 1064 nm using either 3 m of fiber pumped continuously or 1.5 m pumped in the QCW regime. (**a**) Output power in the case of CW pumping (solid curves) and QCW pumping (dashed curves). The onset of SBS was reached at an output power of 25 W and 42.8 W, respectively. (**b**) Normalized optical spectrum in the forward direction under QCW pumping at an output peak power of 42.8 W.

Figure 3a shows the measured dependence of the output power at 1064 nm on the launched pump power for CW and QCW pumping, each for a different fiber length. For a length of 3 m (a small-signal pump absorption of ~21 dB), in both the CW and QCW modes the SBS threshold occurred at a relatively low launched pump power of 38 W. The maximum output power in the CW (average) and QCW (peak power) modes was the same, and both were limited to 25 W by SBS. The slope efficiency was the same (61%). For the 1.5 m length, the output power in the CW mode was limited to 27.6 W by the available pump power, while in the QCW mode, the output peak power was limited by SBS to a value of 42.8 W. Further shortening of the fiber is not a viable option as the slope efficiency would be too low and the increase in output power would be insignificant. The stability of the output power of the fiber amplifier was measured in the CW mode over a period of 1 h. Power fluctuations of less than 0.1% were observed, and no long-term power degradation was noticed.

Figure 3b shows the measured optical spectrum in the forward direction under QCW pumping of a 1.5-m fiber at the maximum output peak power of 42.8 W. The SNR exceeded 55 dB, and the power in the amplified spontaneous emission signal was found to be negligible.

3.3. Second-Harmonic Generation Using an Efficient Nonlinear Crystal

The frequency conversion efficiency of CW 1064 nm in PPLN crystals has been shown to saturate when the output power generated at 532 nm exceeds 3 W [10,16–18,27]. Therefore, our second-harmonic generation is performed only in the QCW mode. To frequency-double the signal at 1064 nm, the laser beam coming out of the amplifier was collimated, then focused into the non-linear crystal using a lens with a focal length of either 100 mm or 150 mm to achieve different beam waist diameters, namely of ~52 µm and ~80 µm, respectively. The nonlinear crystal used was a z-cut, type-0 ee-e 10 mm-long, 1 mm-thick, and 10 mm-wide MgO:PPLN bulk crystal (Covesion, UK) with five periodically poled gratings with periods of 6.83 µm, 6.86 µm, 6.90 µm, 6.93 µm, and 6.96 µm. The following results were obtained with the first grating because it was designed to operate at the lowest phase-matching temperatures, namely 35 °C at 1064 nm. The oven then did not have to be operated at high temperatures. Both the input and output facets of the crystal were coated to reduce their power reflectivity at 532 nm and 1064 nm to less than 1%.

To achieve efficient SHG, the phase-matching temperature proprieties were studied by determining the phase-matching temperature and acceptance bandwidth for each grating.

The measured temperature tuning curve of the single-pass SHG is shown in Figure 4a. The sinc^2 fit to the experimental data shows a full-width at half maximum (FWHM) bandwidth of 3.8 ± 0.4 °C at a phase-matching temperature of 36 °C evaluated at 4 W. This value is slightly larger than the calculated value of the temperature acceptance bandwidth, namely 2.28 °C, using eq. 44 in [28]. This discrepancy may be due to the non-uniformity of the grating period along the length of the crystal, or to uncertainties on the Sellmeier coefficients used to perform the fit [29]. No change in the phase-matching temperature was observed when increasing the fundamental power.

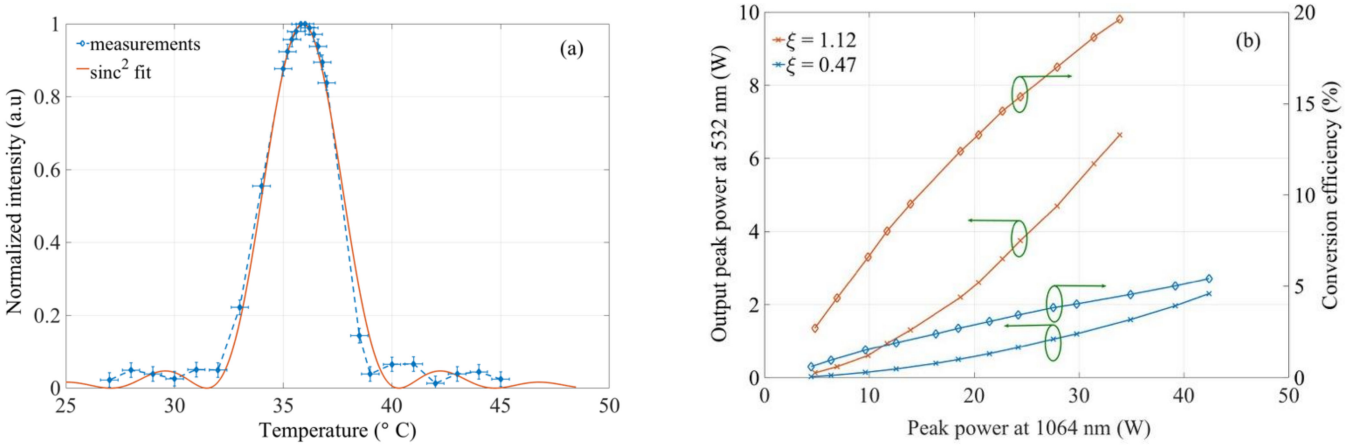

Figure 4. (**a**) Measured temperature tuning curve (with error bars) and sinc^2 fit of the 10-mm MgO:PPLN crystal at 4 W. (**b**) Measured output power at 532 nm as a function of peak pump power at 1064 nm (1% duty cycle) at the output of the 10-mm PPLN crystal, for a fundamental beam with a waist diameter of either ~80 μm or ~52 μm, which corresponds to a focusing parameter ξ of ~1.12 and ~0.47, respectively.

The power conversion efficiency for second-harmonic generation is proportional to the focusing parameter $\xi = L/b$, where L is the length of the nonlinear crystal and b is the confocal parameter [30]. The confocal parameter is defined as $b = 2\pi n_\omega / \lambda_\omega w^2$, where n_ω, λ_ω, and w are the refractive index, wavelength, and beam waist radius, respectively, of the fundamental beam. For this crystal length, the calculated optimum focusing parameter is $\xi \approx 2.84$, which would require a relatively small beam waist diameter of ~32 μm. For peak powers greater than 40 W, this spot size would exceed the damage threshold of the crystal in the CW mode (500 kW/cm^2) and may approach the damage threshold in the QCW mode (no data are reported for the crystal damage in the μs regime). Therefore, we limited our experiments to larger focused beam diameters, namely ~80 μm and ~52 μm, corresponding to an L/b of ~0.47 and ~1.12, respectively. For a 52-μm beam diameter, the conversion efficiency was consequently halved compared to what it would have been if operated at the optimal focusing parameter.

The output peak powers and conversion efficiency measured with respect to the peak power at 1064 nm (duty cycle of 1%) at these beam diameters are presented in Figure 4b. For a beam waist diameter of ~80 μm ($\xi \approx 0.47$), we achieved a maximum output peak power of 2.3 W at 532 nm, which corresponds to a power conversion efficiency of 5.4%. By reducing the beam waist diameter to ~52 μm ($\xi \approx 1.12$), the maximum output peak power and conversion efficiency increased to 6.7 W and 20%, respectively, limited by the PPLN-crystal damage threshold. This corresponds to maximum pulse energies at 532 nm of 230 μJ and 670 μJ for beam diameters of ~80 μm and ~52 μm, respectively, using a pulse duration of 100 μs and a 1% duty cycle (0.1-kHz repetition rate).

No limitations due to thermal effects under these conditions were observed, indicating that further power scaling is feasible for shorter pulse durations. Higher output peak powers at 532 nm can be achieved under similar operating conditions, for example by

using a crystal in a double-pass scheme, a longer nonlinear crystal, or two crystals in a single-pass scheme.

4. Conclusions

We have demonstrated the second-harmonic generation of the fundamental free-space beam generated by a compact single-frequency diode-pumped Yb-doped fiber amplifier operating in the QCW mode. The SHG was achieved in a 10-mm periodically poled MgO-doped $LiNbO_3$ crystal used in a single-pass configuration. By operating the pump diode in the QCW mode with a duty cycle of 1% (100 µs pulses at 100 Hz), it was possible to apply twice as much maximum drive current to the pump laser, thereby increasing by the same amount the maximum available fundamental peak power. The power conversion efficiency of 20% and pulse energies up to 670 µJ were achieved, which can be useful in high-resolution spectroscopy, remote sensing, and holography applications. Moreover, this laser source could prove useful for the generation of high output peak power laser sources operating at 355 nm via frequency tripling.

Author Contributions: Conceptualization, E.B. and M.E.; methodology, E.B. and M.E.; investigation, E.B. and M.E.; writing—original draft preparation, E.B.; writing—review and editing, E.B., M.J.F.D.; supervision, M.E., M.J.F.D., and H.-E.N. All authors have read and agreed to the published version of the manuscript.

Funding: EU Regional funds (135790); Knowledge Foundation (KKS); Region Västernorrland (0868895).

Institutional Review Board Statement: Not applicable.

Informed Consent Statement: Not applicable.

Data Availability Statement: Data is available on request.

Acknowledgments:

Conflicts of Interest: The authors declare no conflict of interest.

References

1. Jones, R.R.; Hooper, D.C.; Zhang, L.; Wolverson, D.; Valev, V.K. Raman Techniques: Fundamentals and Frontiers. *Nanoscale Res. Lett.* **2019**, *14*, 231. [CrossRef] [PubMed]
2. Sharma, S.K.; Misra, A.K.; Lucey, P.G.; Lentz, R.C. A combined remote Raman and LIBS instrument for characterizing minerals with 532 nm laser excitation. *Spectrochim. Acta Part A Mol. Biomol. Spectrosc.* **2009**, *73*, 468–476. [CrossRef] [PubMed]
3. Gallo, E.C.A.; Cantu, L.M.L.; Duschek, F. RDX remote Raman detection on NATO SET-237 samples. *Eur. Phys. J. Plus* **2021**, *136*, 1–11. [CrossRef]
4. Tuschel, D. Selecting an Excitation Wavelength for Raman Spectroscopy. *Spectroscopy* **2016**, *31*, 14–23. Available online: https://www.spectroscopyonline.com/view/selecting-excitation-wavelength-raman-spectroscopy (accessed on 1 March 2016).
5. Balliu, E.; Engholm, M.; Nilson, H.-E. A compact, single-frequency, high-power, SBS-free, Yb-doped single-stage fiber amplifier. In *Solid State Lasers XXVIII: Technology and Devices*; International Society for Optics and Photonics: Bellingham, WA, USA, 2019; Volume 10896, p. 1089618. [CrossRef]
6. Zervas, M.N. Transverse mode instability, thermal lensing and power scaling in Yb3+-doped high-power fiber amplifiers. *Opt. Express* **2019**, *27*, 19019–19041. [CrossRef]
7. Balliu, E.; Engholm, M.; Digonnet, M.J.F.; Coetzee, R.S.; Elgcrona, G.; Nilsson, H.-E. Compact Single-Frequency MOPA Using a Silica Fiber Highly Doped with Yb^{3+}. *Appl. Sci.* **2021**, *11*, 9951. [CrossRef]
8. Agrawal, G. *Nonlinear Fiber Optics*, 5th ed.; Elsevier: Waltham, MA, USA, 2013; pp. 355–384.
9. Boyd, R.W. *Nonlinear Optics*, 3rd ed.; Elsevier: San Diego, CA, USA, 2008; pp. 429–471.
10. Miller, G.D.; Batchko, R.G.; Tulloch, W.M.; Weise, D.R.; Fejer, M.M.; Byer, R.L. 42%-efficient single-pass cw second-harmonic generation in periodically poled lithium niobite. *Opt. Lett.* **1997**, *22*, 1834–1836. [CrossRef]
11. Kumar, S.C.; Samanta, G.K.; Devi, K.; Ebrahim-Zadeh, M. High-efficiency, multicrystal, single-pass, continuous-wave second harmonic generation. *Opt. Express* **2011**, *19*, 11152–11169. [CrossRef]
12. Zhang, K.; Chen, F.; Pan, Q.; Yu, D.; He, Y. Theoretical study on thermal characteristic of MgO:PPLN crystal in high power optical parametric oscillator. *Optik* **2019**, *178*, 190–196. [CrossRef]
13. Furuya, H.; Morikawa, A.; Mizuuchi, K.; Yamamoto, K. High-Beam-Quality Continuous Wave 3 W Green-Light Genera-tion in Bulk Periodically Poled MgO:$LiNbO_3$. *Jpn. J. Appl. Phys.* **2006**, *45*, 6704–6707. [CrossRef]

14. Lai, J.-Y.; Hsu, C.-S.; Hsu, C.-W.; Wu, D.-Y.; Wu, K.; Chou, M.-H. Single pass 7 watts continuous wave 532 nm generation by focusing optimized second harmonic generation in MgO:PPLN. *Proc. SPIE* **2019**, *10902*, 1090205.
15. Mizushima, T.; Furuya, H.; Shikii, S.; Kusukame, K.; Mizuuchi, K.; Yamamoto, K. Second Harmonic Generation with High Conversion Efficiency and Wide Temperature Tolerance by Multi-Pass Scheme. *Appl. Phys. Express* **2008**, *1*, 1. [CrossRef]
16. Qian, Y.; Zhang, L.; Jiang, H.; Cui, S.; Zhou, J.; Feng, Y. 2 W single-frequency, low-noise 509 nm laser via single-pass fre-quency doubling of an ECDL-seeded Yb fiber amplifier. *Appl. Opt.* **2018**, *57*, 8733–8737. [CrossRef]
17. Kang, Y.; Yang, S.; Brunel, M.; Cheng, L.; Zhao, C.; Zhang, H. Second-harmonic generation of a dual-frequency laser in a MgO:PPLN crystal. *Appl. Opt.* **2017**, *56*, 2968–2972. [CrossRef]
18. Rota-Rodrigo, S.; Gouhier, B.; Dixneuf, C.; Antoni-Micollier, L.; Guiraud, G.; Leandro, D.; Lopez-Amo, M.; Traynor, N.; Santarelli, G. Watt-level green random laser at 532 nm by SHG of a Yb-doped fiber laser. *Opt. Lett.* **2018**, *43*, 4284–4287. [CrossRef]
19. Furukawa, Y.; Kitamura, K.; Alexandrovski, A.; Route, R.K.; Fejer, M.M.; Foulon, G. Green-induced infrared absorption in MgO doped LiNbO3. *Appl. Phys. Lett.* **2001**, *78*, 1970–1972. [CrossRef]
20. Ould-Hamouda, A.; Tokoro, H.; Ohkoshi, S.-I.; Freysz, E. Single-shot time resolved study of the photo-reversible phase transi-tion induced in flakes of Ti3O5 nanoparticles at room temperature. *Chem. Phys. Lett.* **2014**, *608*, 106–112. [CrossRef]
21. Lutey, A.H.A.; Ascari, A.; Fortunato, A.; Romoli, L. Long-pulse quasi-CW laser cutting of metals. *Int. J. Adv. Manuf. Technol.* **2017**, *94*, 155–162. [CrossRef]
22. Sonnenfroh, D.M.; Rawlins, W.T.; Allen, M.G.; Gmachl, C.; Capasso, F.; Hutchinson, A.L.; Sivco, D.L.; Baillargeon, J.N.; Cho, A.Y. Application of balanced detection to absorption measurements of trace gases with room-temperature, quasi-cw quan-tum-cascade lasers. *Appl. Opt.* **2001**, *40*, 812–820. [CrossRef]
23. Mehner, E.; Steinmann, A.; Hegenbarth, R.; Braun, B.; Giessen, H. Stable MHz-Repetition-Rate Passively Q-Switched Microchip Laser Frequency Doubled by MgO:PPLN. *Appl. Phys. B* **2012**, *112*, 231–239. [CrossRef]
24. Zhao, H.; Sukhoy, K.; Lima, I.T., Jr.; Major, A. Generation of green second harmonic with 60% conversion efficiency from a Q-switched microchip laser in MgO:PPLN crystal. *Laser Phys. Lett.* **2012**, *9*, 355–358. [CrossRef]
25. Avdokhin, A.; Gapontsev, V.; Kadwani, P.; Vaupel, A.; Samartsev, I.; Platonov, N.; Yusim, A.; Myasnikov, D. High Average Power Quasi-CW Single-Mode Green and UV Fiber Lasers. In *Nonlinear Frequency Generation and Conversion: Materials, Devices, and Applications XIV*; International Society for Optics and Photonics: Bellingham, WA, USA, 2015; Volume 9347, p. 934704. [CrossRef]
26. Suzudo, T.; Satoh, Y.; Hiroi, M.; Mifune, H.; Sato, Y.; Ishizuki, H.; Taira, T.; Nakamura, O.; Watanabe, S.; Furukawa, Y. Diode-pumped Nd:$GdVO_4$ Microchip Laser with a Single-Pass Green Generation in PPMgLN. In *Advanced Solid-State Photonics*; Optical Society of America: Washington, DC, USA, 2007; Paper TuC3.
27. Kontur, F.; Dajani, I.; Lu, Y.; Knize, R.J. Frequency-doubling of a CW fiber laser using PPKTP, PPMgSLT, and PPMgLN. *Opt. Express* **2007**, *15*, 12882–12889. [CrossRef]
28. Fejer, M.; Magel, G.; Jundt, D.; Byer, R. Quasi-phase-matched second harmonic generation: Tuning and tolerances. *IEEE J. Quantum Electron.* **1992**, *28*, 2631–2654. [CrossRef]
29. Gayer, O.; Sacks, Z.; Galunand, E.; Arie, A. Temperature and wavelength dependent refractive index equations for MgO-doped congruent and stoichiometric $LiNbO_3$. *Appl. Phys. B* **2008**, *91*, 343–348. [CrossRef]
30. Boyd, G.D.; Kleinman, D.A. Parametric interaction of focused Gaussian light beams. *J. Appl. Phys.* **1968**, *39*, 3597–3639. [CrossRef]